IET Power Electronics

Research Article

Experimental design of the adaptive backstepping control technique for single-phase shunt active power filters

ISSN 1755-4535
Received on 8th May 2016
Revised 21st February 2017
Accepted on 1st March 2017
E-First on 22nd March 2017
doi: 10.1049/iet-pel.2016.0366
www.ietdl.org

Mahdi Salimi[1] ✉, *Jafar Soltani*[2], *Adel Zakipour*[3]
[1]*Department of Engineering, Ardabil Branch, Islamic Azad University, Ardabil, Iran*
[2]*Department of Engineering, Khomeinishahr Branch, Islamic Azad University, Isfahan, Iran*
[3]*Department of Engineering, Sarab Branch, Islamic Azad University, Sarab, Iran*
✉ *E-mail: m.salimi@iauardabil.ac.ir*

Abstract: In this study, a cascade two-loop non-linear controller is developed for single-phase shunt active power filters which is robust and stable in a wide range of output current and DC-link voltage changes. A variable structure proportional–integral controller is designed to regulate DC-link voltage in the outer loop. Also filter output current is controlled in the inner loop using adaptive backstepping approach. All of the model uncertain parameters are estimated using designed estimation rules. By introduction of suitable Lyapunov functions, proposed controller stability is investigated using Barbalat lemma. Grid reference current is calculated indirectly using a phase-locked loop circuit according to DC-link voltage error. Designed active power filter has been implemented using TMS320F28335 digital signal processor and practical response of the developed controller is studied in some tests. It is shown that the proposed controller is able to eliminate harmonic components of the local load current with a fast dynamic response. Also, compensation capability of the designed non-linear approach is compared with sliding mode controller in similar conditions.

1 Introduction

According to widespread use of power electronics converters in recent years, applications of the non-linear loads have been increased dramatically on electric power grid. It is well known that the presence of current harmonics in power grid may lead to reduction of voltage quality at point of common coupling (PCC). For this reason, electric consumers, which are located in the neighbourhood of non-linear loads will be affected by harmonics. Load current harmonics can be filtered easily by using conventional passive filters. In spite of simple design, high volume and resonance problems are the main disadvantages of the passive filters. In addition, it is not possible to tune a given passive filter for different harmonic components.

In recent years, grid connected inverters (GCIs) have found various applications in photovoltaic systems, wind power generation, online UPSs and so on. The inverter is connected in parallel between the power grid and local loads. In addition to active power exchange, GCI is capable of local loads compensation. If the GCI is employed only for load compensation, a separate active power source is not required on the DC side and its voltage can be maintained using a standard electrolyte capacitor. Such application of the GCI is named shunt active power filter (SAPF).

In direct control approach [1], usually SAPF includes three different control blocks. The reference calculation unit performs online calculations of the local loads reactive current and harmonic components. The current control unit applies appropriate switching signals in order that inverter output current follows the reference value. The DC-link voltage control unit adds an active component to the reference current according to corresponding voltage error. In this case and in spite of power loss, inverter input DC voltage can be kept constant in the desired reference value.

Instead of inverter output current control, grid current can be adjusted in indirect approach. Reference current of the grid can be formed according to grid AC voltage so that its amplitude is determined in a separate control loop based on the inverter DC side voltage error [2]. Considering that the SAPF is not capable of active power exchange with the power utility, so if the DC-link voltage is regulated in the desired value and grid current become pure sinusoidal, it can be concluded that the local load harmonic and reactive components are compensated completely. Actually in indirect control method, reference current calculation and DC-link voltage control units are combined together which significantly can reduce required calculations in SAPFs; hence system dynamic response can be improved considerably. In indirect control approach, SAPF includes only two control loops. First, the voltage outer loop which determines grid reference current based on the DC-link voltage error for inner loop. Second, the inner current loop, which controls inverter output current using pulse-width modulation (PWM) switching scheme.

Application of the linear controllers in GCI is completely challenging task due to system non-linearity. Although it is possible to stabilise a linear controller in a certain operating point [3], in a wide range of load current and DC-link voltage changes, stability of the whole system cannot be guaranteed. Hence, application of the non-linear controllers on indirect control of the SAPFs has been studied in the literature [4–7].

For example, a current controller has been designed for inner loop of the single-phase SAPF using exact feedback linearisation in [4]. Such an approach is not based on small-signal approximation and is valid in the whole operating range of the system. However, in [4], reference current is calculated directly from gird AC voltage. Hence, if grid voltage be distorted, the response of the proposed control method would not be acceptable. Similarly, application of the sliding mode controller (SMC) has been reported in [5] for inner loop of the SAPF. In spite of the presence of the low-order harmonics in grid voltage, it is shown that the proposed method can maintain grid current total harmonic distortion (THD) in the acceptable range. However, SMC of [5] has chattering problem as well as considerable steady-state error.

According to the simplicity of the practical implementation and inherent overcurrent protection capability, application of the hysteresis current controller has been studied in inner loop of the SAPFs [6]. However, switching frequency variations complicates selection of the coupling inductor in hysteresis current controllers. Lyapunov-based current control of the single-phase SAPFs has been reported in [7]. Robustness of the controller with respect to load changes has been studied in some simulations. However, it is not possible to estimate uncertain parameters of the system in [7].

Also according to the simulation results, grid current has considerable low-order harmonic components. Although application of the non-linear controllers has been reported for the inner loop of the GCIs, in [3–7], a conventional proportional–integral (PI) controller is employed for reference current calculation in the outer loop. Hence, the stability of the outer loop cannot be guaranteed in a wide operating range.

To reduce converter steady-state error, a multi-resonance SMC has been designed for GCIs [8]. In the proposed method, only active sinusoidal current can be injected from GCI into grid. In [8], DC side of inverter is connected to an independent voltage source and response of the SMC in DC-link voltage regulation has not been studied. For this reason, developed non-linear controller is not suitable for SAPFs.

Considering systematic and recursive design process, some papers are reported on the application of the backstepping controller for GCIs in recent years [9–11]. The designed method in [9] is applicable to both grid connected and stand-alone inverters. In grid connected mode, it is possible to control output active power of the inverter. In fact, the designed inverter of [9] operates as a distributed generator with unity power factor. According to the presence of the low-order harmonics in grid voltage, a phase-locked loop (PLL) is employed for generation of the reference current. However, inverter input voltage is supplied through an independent voltage source and it is assumed to be constant in system model. Hence, designed backstepping controller in [9] is not applicable to SAPFs. Backstepping approach has been developed to control a bidirectional grid connected H-bridge inverter in [10]. In the DC side of the inverter, solar cells are connected as an active power generator. Also, special load (telecommunication equipment) is connected to the DC bus of the system. In the developed controller, extra generated photovoltaic power is injected into the grid through a bridge converter. During night hours, the converter operates in the rectifier mode and supplies the required active power of telecommunication equipment. Although the designed converter is able to exchange active power with the power utility with unity power factor, compensation of the local AC loads is not studied in [10]. Also, the effects of the converter parasitic elements and uncertain parameters have not been studied in modelling and backstepping controller design. To estimate these uncertain parameters, an adaptive backstepping controller has been designed for the inner current loop of the SAPF in [11]. In this reference, backstepping and adaptive fuzzy controllers have been combined to reduce effect of external disturbances and model uncertainties. However, in [11], it is not possible to estimate all of the model uncertain parameters. In fact, uncertain parameters that are multiplied into the control effort cannot be estimated using the mentioned fuzzy backstepping. These parameters are coupling inductance and its equivalent series resistance.

In this paper, a two-loop non-linear cascade controller is designed for single-phase SAPFs. The adaptive backstepping controller is developed to control output current of the filter in an inner loop. All of the model uncertain parameters can be estimated using proposed adaptive controller. Furthermore, inverter input DC voltage is regulated in the outer loop using a variable structure (VS) PI controller. Benefits of the both VS and linear controllers are combined in the outer loop of the designed controller. Obviously, according to application of the non-linear controllers in both inner and outer loops, developed SAPF is stable and robust in a wide range of operation. To reduce the effect of power system voltage distortion in load compensation, a single-phase PLL is employed in the outer loop to generate a pure sinusoidal waveform which is in phase with grid voltage.

2 System model

The single-phase SAPF is shown in Fig. 1 considering H-bridge inverter. It is assumed that the inverter is switched using bipolar PWM technique. Switching signal (x_g) is obtained by comparison of a high frequency sawtooth waveform (v_{tri}) with the desired AC control signal (v_{control}). In spite of control signal variations, it can be assumed almost constant in a switching cycle (T) due to very higher frequency of the sawtooth waveform. Considering Appendix 1, averaged state-space model of system can be expressed as

$$\begin{pmatrix}\dot{x}_1\\ \dot{x}_2\end{pmatrix} = \begin{pmatrix}\theta_1 & -\theta_2 u\\ \theta_3 u & 0\end{pmatrix}\begin{pmatrix}x_1\\ x_2\end{pmatrix} + \begin{pmatrix}\theta_2 v_s\\ 0\end{pmatrix} \tag{1}$$

where in this equation, $\theta_1 = -(r_{\text{L}} + 2r/L)$, $\theta_2 = (1/L)$ and $\theta_3 = (1/C)$ are uncertain parameters of the system. Also, u is the amplitude modulation index of the inverter. Moreover, $\boldsymbol{X} = (x_1, x_2)^{\text{T}} = (i_{\text{F}}, v_{\text{DC}})^{\text{T}}$ is state vector of the control system. Considering state-space equations, dynamic model of the single-phase SAPF is shown in Fig. 2*a*.

3 Controller design

As shown in Fig. 2*b*, a VS PI (VS-PI) controller is cascaded with an adaptive backstepping controller for obtaining unity power factor in a single-phase SAPF. This combined controller purely filters out the loads current harmonics. In fact, harmonic components are taken from the main and transferred to the SAPF. In this condition, grid current would be completely sinusoidal and in phase with the utility voltage

$$i_s^* = i_s = k \sin\theta \tag{2}$$

In this equation, k is a constant coefficient, which depends on local load active power consumption. Also i_s^* is reference value of the grid current. As it is explained in the next section, $\sin\theta$ is generated using a single-phase PLL. The value of the k can be determined in an outer loop according to DC-link voltage error.

The VS-PI controller generates the fundamental reference current that is absorbed by the non-linear load. That can be achieved by online adjustment of the DC-link voltage on a constant reference value. It should be noted that a small part of the fundamental current taken from the main is absorbed by the voltage source SAPF to cover the power losses and the rest of the fundamental current is forwarded to the non-linear load.

3.1 Outer-loop design

This loop adjusts grid reference current (i_s^*) and subsequently determines filter reference current (i_{F}^*) so that the DC-link voltage be equal to its reference value (v_{DC}^*). Referring to [12], VS-PI controller consists of a first-order derivative type sliding mode controller in parallel with a linear conventional PI controller as shown in Figs. 2*b* and *c*. Sliding mode controller is defined by a switching surface as

$$s_V = (v_{\text{DC}}^* - v_{\text{DC}}) + \alpha \frac{\mathrm{d}(v_{\text{DC}}^* - v_{\text{DC}})}{\mathrm{d}t} = e_v + \alpha \frac{\mathrm{d}e_v}{\mathrm{d}t} \tag{3}$$

or in Laplace domain $S_V = e_v + \alpha e_v s$. Design positive constant α is selected in a manner to impose the desired linear first-order behaviour of the system during sliding mode when $s_V = 0$. The VS-PI controller produces the factor k for generation of the fundamental reference current that is observed by the non-linear load

$$k = [e_v + K_{\text{VSC}}\,\text{sgn}(S_V)]\left(K_{\text{P}} + \frac{K_{\text{I}}}{s}\right) \tag{4}$$

where K_{P} and K_{I} are the PI controller gains and α and K_{VSC} are gains of the VS controller. In [12], VS controller is named 'linear and variable structure control'. This controller is generalised and flexible scheme which takes the advantages and features of the linear controller (smooth operation) and VS controller (robustness to perturbation and model uncertainties). As discussed above, the VS-PI controller in (4) employs a switching component and a

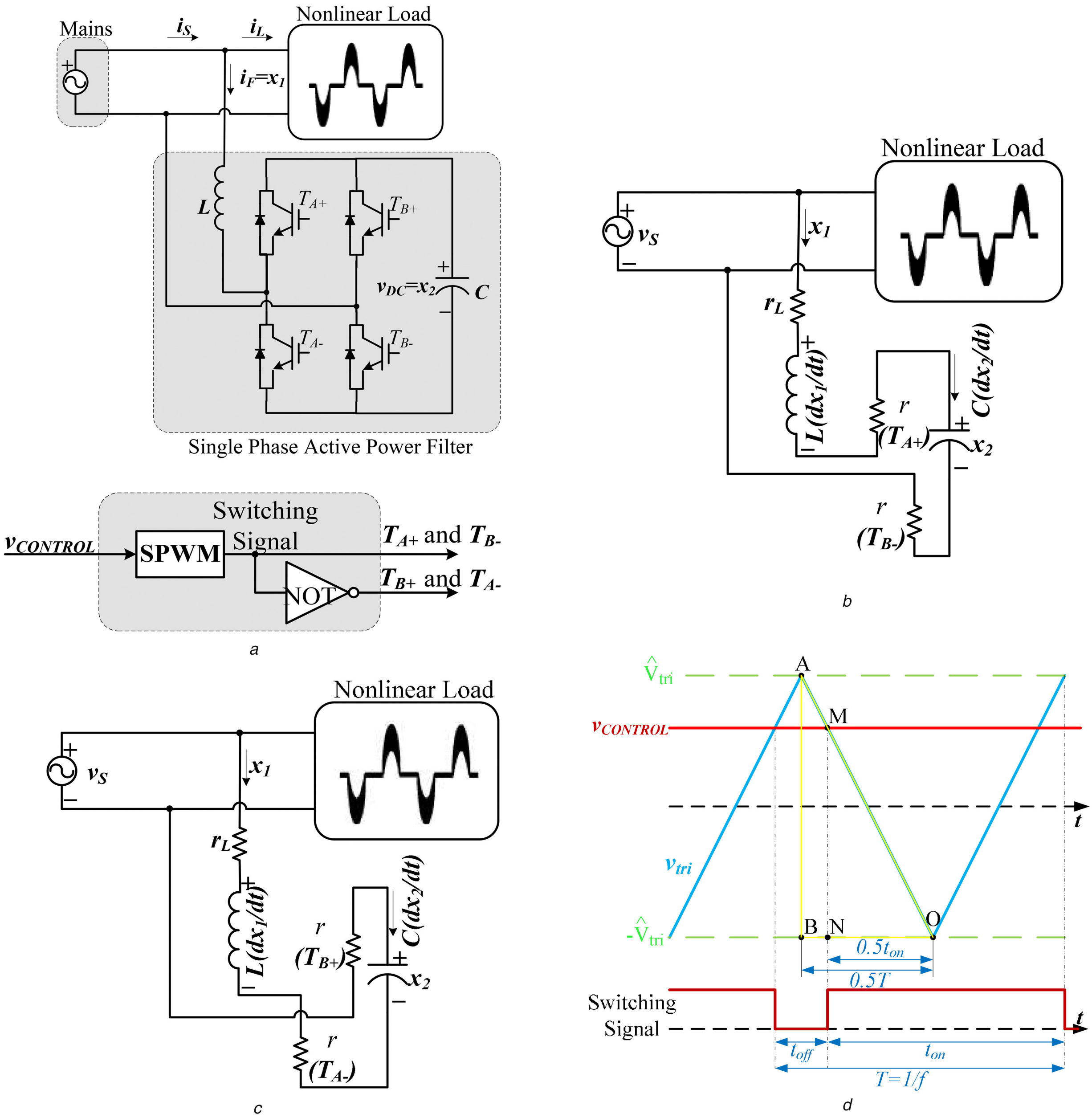

Fig. 1 *Single-phase SAPF circuit and PWM controller*
(a) Single-phase SAPF with bipolar PWM, ***(b)*** System equivalent circuit during active state of the switching signal, ***(c)*** System equivalent circuit during inactive state of the switching signal, ***(d)*** Comparison of the triangular and control signals in bipolar PWM

linear one. During transient moments when $e_v \gg K_{\rm VSC}\,\mathrm{sgn}(S_V)$, it is seen that linear PI behaviour is dominant. On the other hand, in steady-state operation, errors are very small and the switching behaviour prevails. Adequate balance between linear and switching behaviours is easily obtained by proper gain selection. PI gains are selected so that the linear controller provides the desired dynamic response while the VS controller gains determine the robustness during steady-state operation. According to VS controller design procedure [12], the gains of the mentioned controller should be large enough to compensate for modelling uncertainties and perturbations. In this case, α and $K_{\rm VSC}$ are selected by trial and error method as large as needed to obtain the desired performance in terms of robustness and chattering.

3.2 Inner controller – current loop design

This controller adjusts converter switching signal to regulate filter output current in its corresponding reference value $i_{\rm F}^* = i_{\rm L} - i_s^* = x_1^*$. In this case, all of the reactive and harmonic components of load current will be supplied by SAPF. Considering non-linear nature of the SAPF, in this paper adaptive backstepping controller has been employed for system inner loop. It is clear that system model parameters are uncertain. So the controller is developed so that all of the model's impedances can be estimated using some appropriate estimation rules. The adaptive backstepping controller for single-phase SAPF is designed in two steps as follows.

First step: Considering filter reference current value (x_1^*), the current error is defined as

$$z_1 = x_1 - x_1^* \tag{5}$$

According to (1) and (5), it is possible to write derivative of the first error variable as

$$\dot{z}_1 = \dot{x}_1 - \dot{x}_1^* \Rightarrow \dot{z}_1 = \theta_1 x_1 - \theta_2 u x_2 + \theta_2 v_s - \dot{x}_1^* \tag{6}$$

Considering uncertain parameters of the model ($\theta_i; i = 1-3$), it is assumed that $\hat{\theta}_i$ is estimation of the ith parameter. Hence, (6) can be rewritten as below:

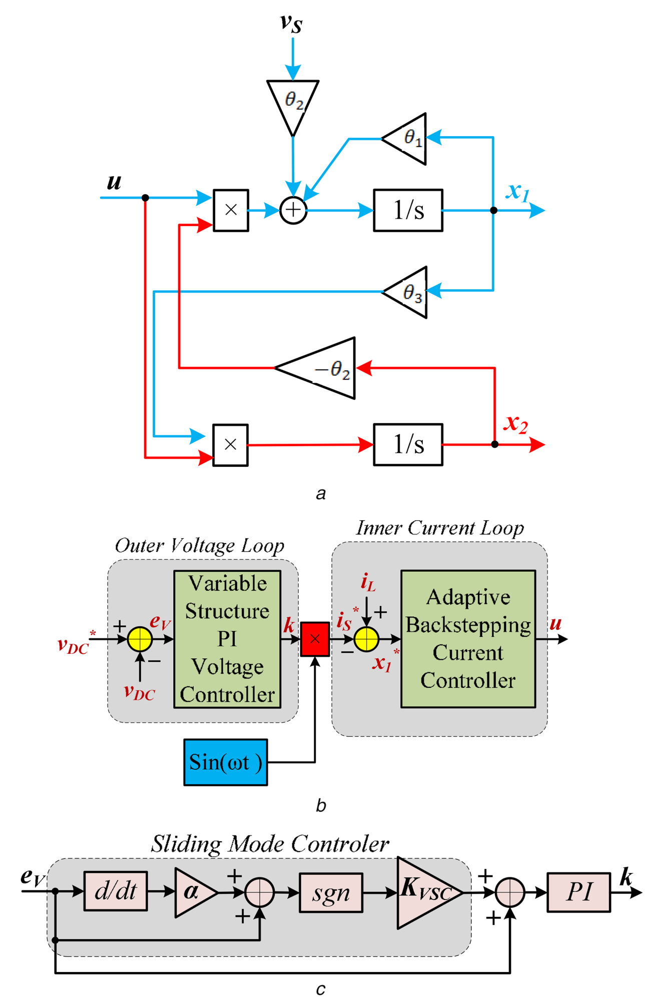

Fig. 2 *Dynamic model and cascade control of the SAPF*
(a) Dynamic model of the single-phase SAPF, ***(b)*** Proposed two loop controller, ***(c)*** VS-PI controller in the outer loop

$$\dot{z}_1 = \hat{\theta}_1 x_1 - \hat{\theta}_2 u x_2 + \hat{\theta}_2 v_s - \dot{x}_1^* + (\theta_1 - \hat{\theta}_1)x_1 \\ -(\theta_2 - \hat{\theta}_2)u x_2 + (\theta_2 - \hat{\theta}_2)v_s \tag{7}$$

By defining the uncertain parameters vector as $\hat{\boldsymbol{\theta}}^{\mathrm{T}} = [\theta_1\ \theta_2\ \theta_3]$, (6) can be rewritten as

$$\dot{z}_1 = \hat{\boldsymbol{\theta}}^{\mathrm{T}}\boldsymbol{\Phi}_1 - \dot{x}_1^* + (\boldsymbol{\theta} - \hat{\boldsymbol{\theta}})^{\mathrm{T}}\boldsymbol{\Phi}_1 \tag{8}$$

where $\boldsymbol{\Phi}_1$ should be defined as

$$\boldsymbol{\Phi}_1^{\mathrm{T}} = [x_1 \quad (-u x_2 + v_s) \quad 0] \tag{9}$$

To investigate stability of the system, first Lyapunov function is defined as

$$V_1 = \frac{1}{2}[z_1^2 + (\boldsymbol{\theta} - \hat{\boldsymbol{\theta}})^{\mathrm{T}}\boldsymbol{\Gamma}^{-1}(\boldsymbol{\theta} - \hat{\boldsymbol{\theta}})] \tag{10}$$

where in this equation, $\boldsymbol{\Gamma}$ is a 3×3 diagonal matrix which diagonal elements are called γ_{ii}. Time derivative of the first Lyapunov function can be obtained as

$$\dot{V}_1 = z_1\dot{z}_1 + \left(\boldsymbol{\theta} - \hat{\boldsymbol{\theta}}\right)^{\mathrm{T}}\boldsymbol{\Gamma}^{-1}(-\dot{\hat{\boldsymbol{\theta}}}) \tag{11}$$

By replacing (8) into (11), the following equation can be obtained as:

$$\dot{V}_1 = z_1(\hat{\boldsymbol{\theta}}^{\mathrm{T}}\boldsymbol{\Phi}_1 - \dot{x}_1^*) + (\boldsymbol{\theta} - \hat{\boldsymbol{\theta}})^{\mathrm{T}}\boldsymbol{\Gamma}^{-1}(-\dot{\hat{\boldsymbol{\theta}}} + \boldsymbol{\Gamma}z_1\boldsymbol{\Phi}_1) \tag{12}$$

In (12), if it is assumed that $(\hat{\boldsymbol{\theta}}^{\mathrm{T}}\boldsymbol{\Phi}_1 - \dot{x}_1^*)$ is equal to $-c_1 z_1$, and $(-\dot{\hat{\boldsymbol{\theta}}} + \boldsymbol{\Gamma}z_1\boldsymbol{\Phi}_1)$ is equal to zero, then $\dot{V}_1 = -c_1 z_1^2$ will be obtained which is a negative semi-definite function and ensures asymptotical stability of the system. In these equations, c_1 is a positive design scalar.

Second step: Considering that $(\hat{\boldsymbol{\theta}}^{\mathrm{T}}\boldsymbol{\Phi}_1 - \dot{x}_1^*)$ maybe not be equal to $-c_1 z_1$, the differences can be defined as the second error variable:

$$z_2 = \hat{\boldsymbol{\theta}}^{\mathrm{T}}\boldsymbol{\Phi}_1 - \dot{x}_1^* - (-c_1 z_1) \tag{13}$$

Derivative of the first error variable can be written by combining (8) and (13) as

$$\dot{z}_1 = -c_1 z_1 + z_2 + (\boldsymbol{\theta} - \hat{\boldsymbol{\theta}})^{\mathrm{T}}\boldsymbol{\Phi}_1 \tag{14}$$

According to (1), (6) and (9), time derivative of the second error variable can be obtained from (13) as

$$\dot{z}_2 = A + \hat{\boldsymbol{\theta}}^{\mathrm{T}}\boldsymbol{\Phi}_2 + (\boldsymbol{\theta} - \hat{\boldsymbol{\theta}})^{\mathrm{T}}\boldsymbol{\Phi}_2 \tag{15}$$

where in this equation

$$A = \dot{\hat{\theta}}_1 x_1 + \dot{\hat{\theta}}_2(-u x_2 + v_s) - \dot{u}\hat{\theta}_2 x_2 + \hat{\theta}_2\dot{v}_s - \ddot{x}_1^* - c_1\dot{x}_1^* \tag{16}$$

$$\boldsymbol{\Phi}_2^{\mathrm{T}} = \left[(\hat{\theta}_1 + c_1)x_1 \quad (\hat{\theta}_1 + c_1)(-u x_2 + v_s) \quad -u^2\hat{\theta}_2 x_2\right] \tag{17}$$

In the second step, Lyapunov function can be considered as follows:

$$V_2 = \frac{1}{2}[z_1^2 + z_2^2 + \left(\boldsymbol{\theta} - \hat{\boldsymbol{\theta}}\right)^{\mathrm{T}}\boldsymbol{\Gamma}^{-1}(\boldsymbol{\theta} - \hat{\boldsymbol{\theta}})] \tag{18}$$

Hence, time derivative of V_2 will be obtained as

$$\dot{V}_2 = z_1\dot{z}_1 + z_2\dot{z}_2 + \left(\boldsymbol{\theta} - \hat{\boldsymbol{\theta}}\right)^{\mathrm{T}}\boldsymbol{\Gamma}^{-1}(-\dot{\hat{\boldsymbol{\theta}}}) \tag{19}$$

By substitution $\dot{z}_1$ and $\dot{z}_2$ from (14) and (15), $\dot{V}_2$ will be simplified as

$$\dot{V}_2 = -c_1 z_1^2 + z_1 z_2 + z_2(A + \hat{\boldsymbol{\theta}}^{\mathrm{T}}\boldsymbol{\Phi}_2) \\ +\left(\boldsymbol{\theta} - \hat{\boldsymbol{\theta}}\right)^{\mathrm{T}}\boldsymbol{\Gamma}^{-1}(-\dot{\hat{\boldsymbol{\theta}}} + \boldsymbol{\Gamma}z_1\boldsymbol{\Phi}_1 + \boldsymbol{\Gamma}z_2\boldsymbol{\Phi}_2) \tag{20}$$

If it is assumed that

$$A + \hat{\boldsymbol{\theta}}^{\mathrm{T}}\boldsymbol{\Phi}_2 = -c_2 z_2 \tag{21}$$

and

$$-\dot{\hat{\boldsymbol{\theta}}} + \boldsymbol{\Gamma}z_1\boldsymbol{\Phi}_1 + \boldsymbol{\Gamma}z_2\boldsymbol{\Phi}_2 = 0 \tag{22}$$

The second Lyapunov function $\dot{V}_2$ will be simplified to $\dot{V}_2 = -c_1 z_1^2 + z_1 z_2 - c_2 z_2^2$. Now, if both design parameters c_1 and c_2 are selected larger than 0.5, time derivative of the second Lyapunov function will be a negative semi-definite function. As a result, it can be concluded that in the developed controller, both error variables z_1 and z_2 are bounded. Stability analysis of the proposed controlled is presented in Appendix 2 according to *Barbalat lemma* [13].

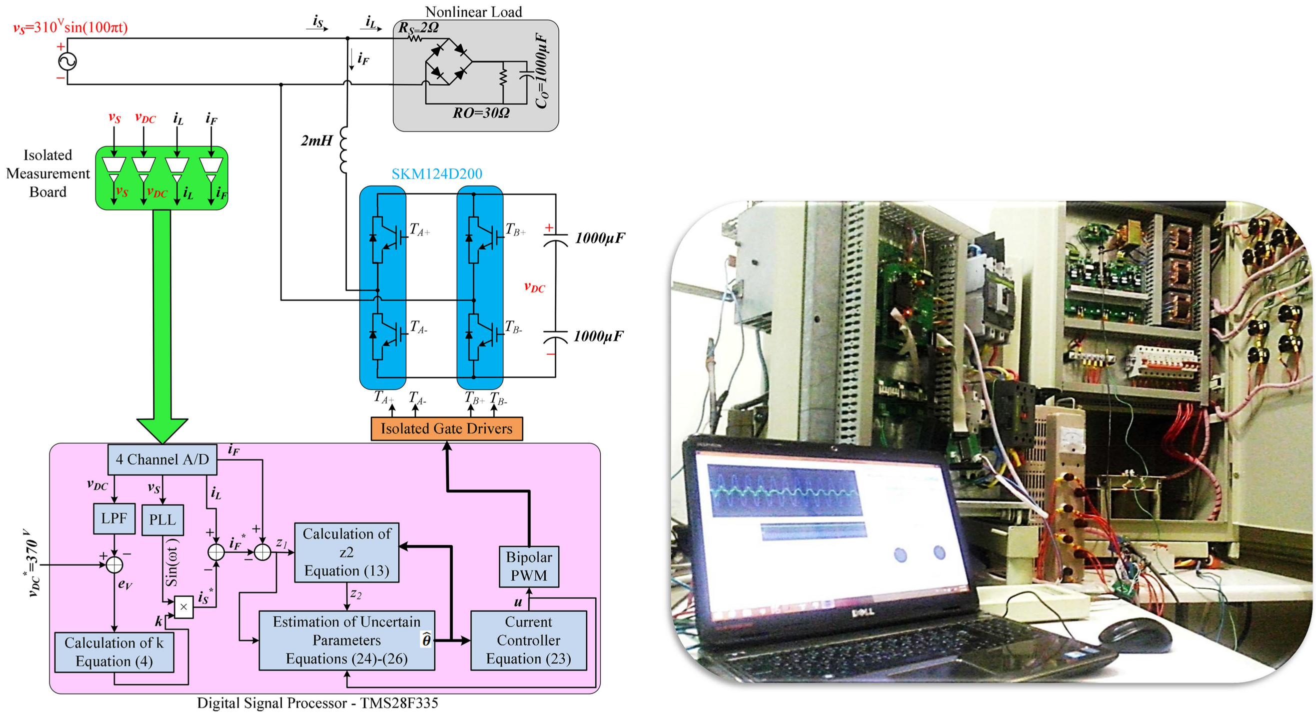

a *b*

Fig. 3 *Implementation of the proposed controller in single-phase SAPF*
(a) Block diagram of the implemented system, ***(b)*** Experimental setup

Final controller law as well as uncertain parameters estimation rules are achieved as below by replacing (9) and (17) into (21) and (22)

$$\dot{u} = \frac{1}{\hat{\theta}_2 x_2}\Big\{x_1\Big[\dot{\hat{\theta}}_1 + \hat{\theta}_1\big(\hat{\theta}_1 + c_1\big) + c_2\hat{\theta}_1 + c_1c_2 - u^2\hat{\theta}_2\hat{\theta}_3\Big]$$
$$+x_2\Big[-u\dot{\hat{\theta}}_2 - u\hat{\theta}_2\big(\hat{\theta}_1 + c_1\big) - c_2\hat{\theta}_2 u\Big]$$
$$+v_s\Big[\dot{\hat{\theta}}_2 + \hat{\theta}_2\big(\hat{\theta}_1 + c_1\big) + c_2\hat{\theta}_2\Big] + \hat{\theta}_2\ddot{v}_s - \ddot{x}_1^* - (c_1 + c_2)\dot{x}_1^* - c_1c_2x_1^*\Big\} \tag{23}$$

$$\dot{\hat{\theta}}_1 = \gamma_{11}x_1[z_1 + z_2(\hat{\theta}_1 + c_1)] \tag{24}$$

$$\dot{\hat{\theta}}_2 = \gamma_{22}(-ux_2 + v_s)[z_1 + z_2(\hat{\theta}_1 + c_1)] \tag{25}$$

$$\dot{\hat{\theta}}_3 = \gamma_{33}x_1[z_1(-u^2\hat{\theta}_2)] \tag{26}$$

4 Experimental results

The single-phase SAPF is implemented based on the proposed non-linear controllers as well as uncertain parameters estimation rules in (23)–(26). Circuit topology, nominal values of the system, controller block diagram and experimental setup are illustrated in Fig. 3. A single-phase rectifier with RC load is employed as a non-linear load. The presented controller has been implemented using a digital signal processor (DSP-TMS28F335) from Texas Instruments. Both switching and sampling frequencies of system are 34 kHz.

Measurement of the filter and load currents are performed using Hall-effect LEM sensors. Different gains of controller have been adjusted so that dynamic and steady-state responses of the system are acceptable in different operational conditions. Considering distorted waveform of the PCC voltage, a PLL circuit is employed for reference current generation. To improve system performance, a notch filter is used in the PLL phase detector output. The cutoff frequency of the notch filter is twice of the grid frequency (100 Hz). Design details of the employed PLL are given in [14]. As it is shown in Fig. 4*a*, in spite of the presence of significant harmonics in grid voltage, output of the designed PLL circuit is pure sinusoidal and in phase with PCC voltage.

4.1 Test I: Steady-state operation

PCC voltage (v_s) and non-linear load current (i_L) waveforms are illustrated in Fig. 4*b*. Also, harmonic spectrum of the load current is shown in Fig. 4*c*. It is seen that load current THD is around 51.8%. Furthermore, the grid voltage has considerable harmonics and its THD is more than 5%.

During steady-state operation, the response of the proposed controller is shown in Fig. 5. In this plot, experimental waveforms of the grid and filter currents are illustrated with respect to PCC voltage. As it is shown after compensation, grid current is sinusoidal and in phase with the PCC voltage. Harmonic spectrum of the grid current is given after compensation in Fig. 5*c*. It is seen that the grid current THD is equal to 1.52% using proposed SAPF, which is fully compatible with IEEE standards [15]. Also it is around 3% less than SMC of [5] in similar conditions.

4.2 Test II: Dynamic response of the inner loop

(a) *Startup:* In this test, it is assumed that the inverter DC-link voltage is regulated around its nominal value (370 V) using outer loop. In fact, load current signal is not applied to the inner current control loop before regulation of the DC-link voltage. Finally, load current is applied to the inner current control loop in a specific instant. To investigate dynamic behaviour of the current controller during startup, practical response of the developed controller is shown in Fig. 6. As it is obvious, in spite of considerable load current changes, proposed controller enjoys fast dynamic response.
(b) *Amplitude and phase changes of the reference current:* To evaluate inner loop response in a wide range, different changes are considered in the system load current. In this test, load real current feedback is disconnected and a virtual signal is applied to the controller. Virtual load current feedback has a 90° phase shift with grid voltage (reactive compensation). In Figs. 7*a* and *b*, experimental dynamic response of the proposed current controller with respect to amplitude changes of the virtual load current is shown. Also in Figs. 7*c* and *d*, response of the current controller to phase change of the load is illustrated. It is clear that in spite of load current changes in a wide range, the proposed controller is

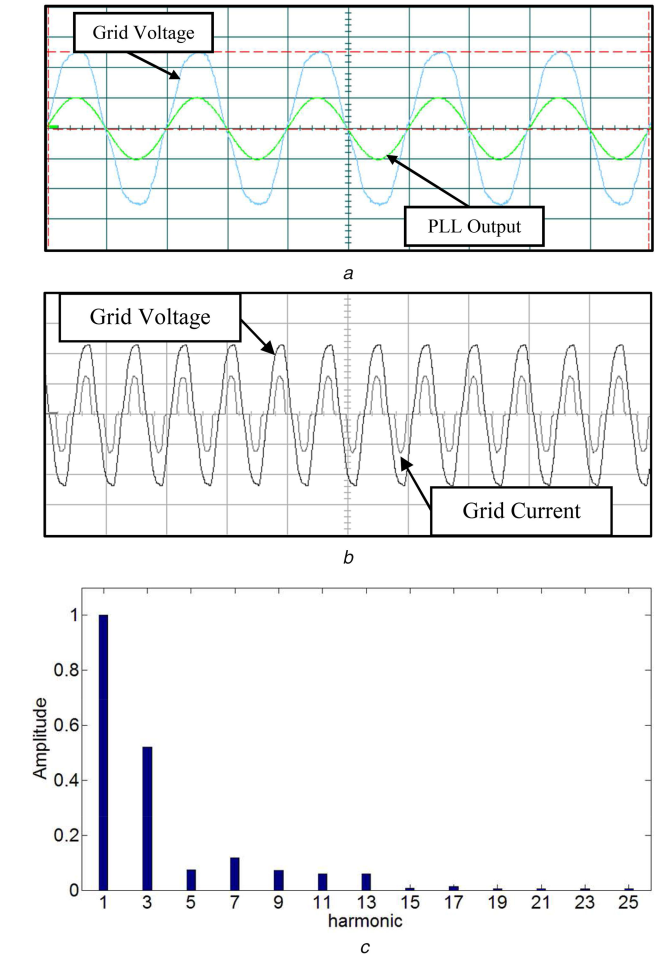

Fig. 4 *Load voltage and current harmonics*
(a) Grid (PCC) voltage and PLL output waveforms, ***(b)*** PCC voltage (v_s) and the non-linear load current (i_L) waveforms (voltage div.: 125 V, current div.: 13 A, time div.: 5 ms), ***(c)*** Load current harmonic spectrum

completely stable and enjoys a fast dynamic response. It is assumed that the DC-link voltage is regulated in its reference value during load current changes.

4.3 Test III: Dynamic response of the outer loop

In Fig. 8, dynamic response of the controller during step changes of the DC-link voltage is presented. It is assumed that during load compensation, DC-link reference voltage is stepped from 370 to 470 V. As shown in Fig. 8, proposed voltage controller is capable of tracking reference value and has a good dynamic response. Also during changes of the DC-link voltage, the current loop is completely stable and robust. It should be noted that in all of the practical results: $c_1 = 10000$, $c_2 = 1000$, $\gamma_{ii} = 10^{-6}; i = 1-3$, $K_P = 0.5$, $K_I = 5$, $K_{VSC} = 0.8$ and $\alpha = 0.001$.

5 Conclusion

Non-linear control of the SAPF is studied using adaptive backstepping and VS approaches. DC-link voltage is regulated by definition of the suitable reference signal for current controller. Using TMS320F28335 digital signal processor, proposed SAPF is implemented. Accuracy and effectiveness of the designed non-linear controller are evaluated considering different practical tests. It is shown that the developed controller is robust and stable in a wide range of output current and DC-link voltage changes. Also, dynamic response of the SAPF is completely fast during step changes of the reference current. After filter startup, full compensation of the local non-linear load is accomplished in 10 ms which is equal to half of the grid voltage period. In spite of

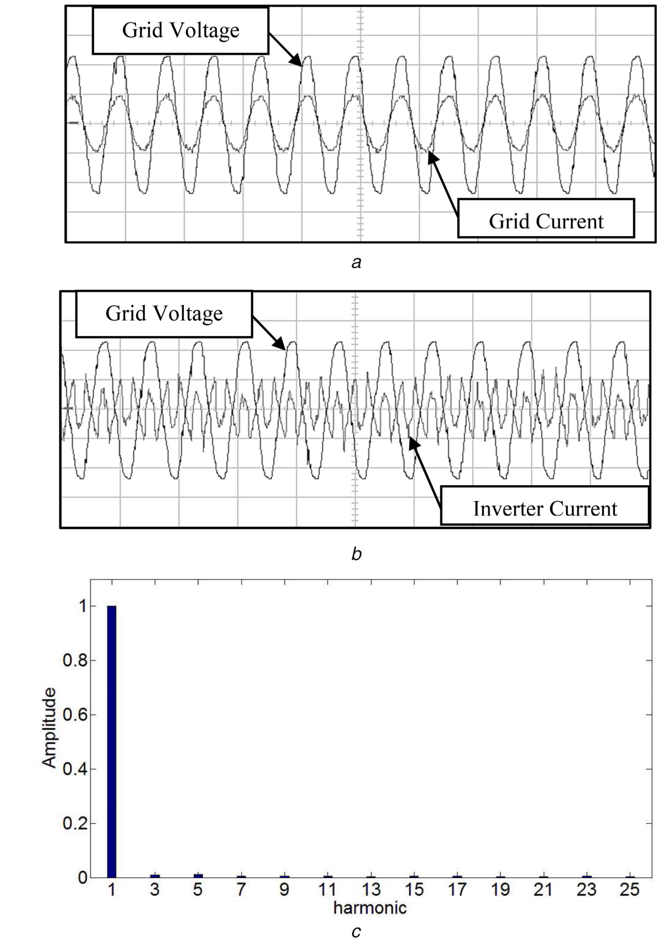

Fig. 5 *Steady-state response of the proposed SAPF*
(a) Grid voltage and current waveforms (voltage div.: 125 V, current div.: 13 A, time div.: 25 ms), ***(b)*** Filter current and grid voltage waveforms (voltage div.: 125 V, current div.: 8.5 A, time div.: 25 ms), ***(c)*** Harmonic spectrum of the grid current

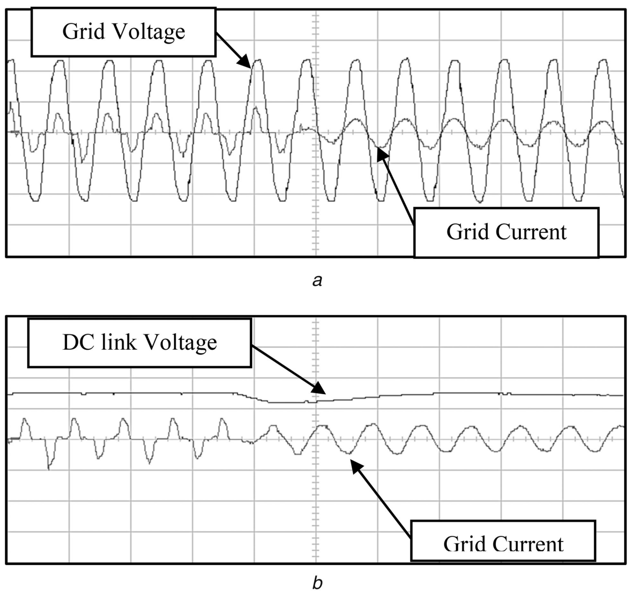

Fig. 6 *Dynamic response of the inner current controller*
(a) Grid voltage and current during system startup (voltage div.: 125 V, current div.: 32.5 A, time div.: 25 ms), ***(b)*** DC-link voltage and grid current during system startup (voltage div.: 250, current div.: 32.5 A, time div.: 25 ms)

applying a local load with relatively high THD value (around 52%), proposed controller is able to keep THD of the grid current in the standard range (around 1.5%). It is shown that THD of the grid current in the developed adaptive backstepping controller is 3% less than SMC in similar conditions.

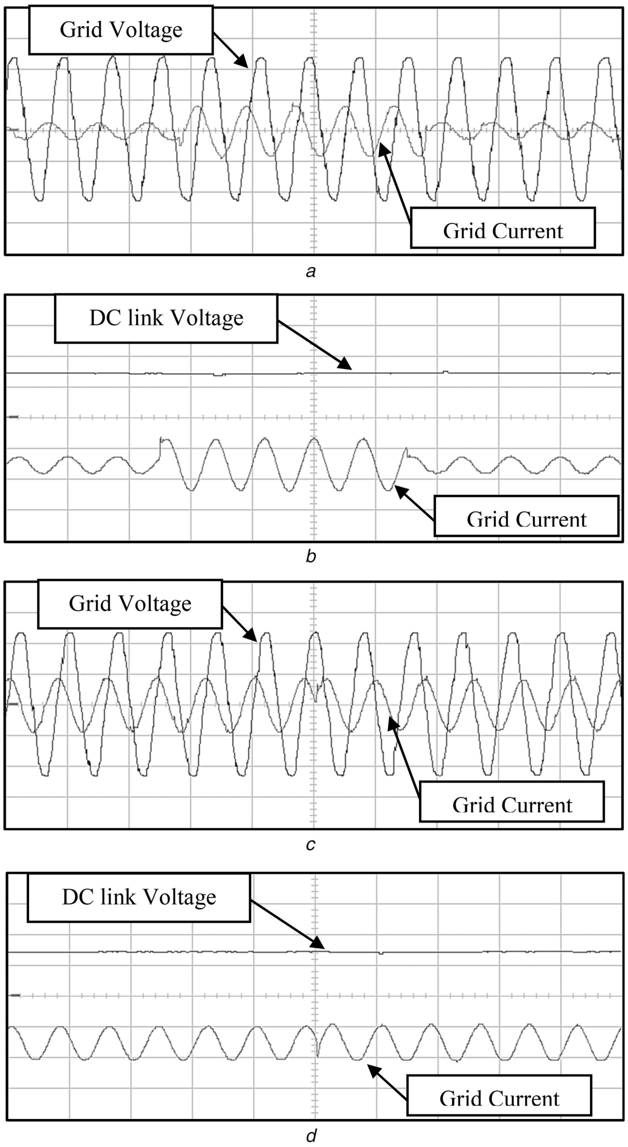

Fig. 7 *Response of the proposed controller during load current changes*
(a) Grid voltage and output current of the SAPF during load current amplitude changes (voltage div.: 125 V, current div.: 32.5 A, time div.: 25 ms), ***(b)*** DC-link capacitor voltage and output current of the SAPF during load current amplitude changes (voltage div.: 250, current div.: 32.5 A, time div.: 25 ms), ***(c)*** Grid voltage and output current of the SAPF during load current phase changes (voltage div.: 125 V, current div.: 32.5 A, time div.: 25 ms), ***(d)*** DC-link capacitor voltage and output current of the SAPF during load current phase changes (voltage div.: 250, current div.: 32.5 A, time div.: 25 ms)

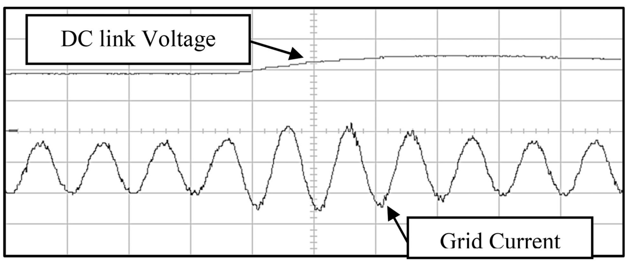

Fig. 8 *DC-link voltage and output current of the SAPF during step changes of the DC-link voltage reference from 370 to 470 V (voltage div.: 200, current div.: 32.5 A, time div.: 20 ms)*

6 Acknowledgments

This research was supported by the Islamic Azad University – Ardabil Branch under Research Grant.

7 References

[1] Wang, L., Lam, C.-S., Wong, M.-C., *et al.*: 'Non-linear adaptive hysteresis band pulse-width modulation control for hybrid active power filters to reduce switching loss', *IET Power Electron.*, 2015, **8**, (11), pp. 2156–2167
[2] Singh, B.N.: 'Sliding mode control technique for indirect current controlled active filter'. IEEE Region 5, 2003 Annual Technical Conf., 11 April 2003, pp. 51–58
[3] Rahmani, S., Mendalek, N., Al-Haddad, K.: 'Experimental design of a nonlinear control technique for three-phase shunt active power filter', *IEEE Trans. Ind. Electron.*, 2010, **57**, (10), pp. 3364–3375
[4] Matas, J., de Vicuna, L.G., Miret, J., *et al.*: 'Feedback linearization of a single-phase active power filter via sliding mode control', *IEEE Trans. Power Electron.*, 2008, **23**, (1), pp. 116–125
[5] Miret, J., de Vicuna, L.G., Castilla, M., *et al.*: 'Design of an analog quasi-steady-state nonlinear current-mode controller for single-phase active power filter', *IEEE Trans. Ind. Electron.*, 2009, **56**, (12), pp. 4872–4881
[6] Mahanty, R.: 'Indirect current controlled shunt active power filter for power quality improvement', *Int. J. Electr. Power Energy Syst.*, 2014, **62**, pp. 441–449
[7] Abouloifa, B., Giri, F., Lachkar, I., *et al.*: 'Cascade nonlinear control of shunt active power filters with average performance analysis', *Control Eng. Pract.*, 2014, **26**, pp. 211–221
[8] Hao, X., Yang, X., Liu, T., *et al.*: 'A sliding-mode controller with multi-resonant sliding surface for single-phase grid-connected VSI with an LCL filter', *IEEE Trans. Power Electron.*, 2013, **28**, (5), pp. 2259–2268
[9] Wai, R.-J., Lin, C.-Y., Wu, W.-C., *et al.*: 'Design of backstepping control for high-performance inverter with stand-alone and grid-connected power-supply modes', *IET Power Electron.*, 2013, **6**, (4), pp. 752–762
[10] Martin, A.D., Cano, J.M., Silva, J.F.A., *et al.*: 'Backstepping control of smart grid-connected distributed photovoltaic power supplies for telecom equipment', *IEEE Trans. Energy Convers.*, 2015, **30**, (4), pp. 1496–1504
[11] Hou, S., Fei, J.: 'Adaptive fuzzy backstepping control of three-phase active power filter', *Control Eng. Pract.*, 2015, **45**, pp. 12–21
[12] Utkin, V., Guldner, J., Shi, J.: '*Sliding mode control in electromechanical systems*' (Taylor & Francis, New York, 1999)
[13] Slotine, J.J.E., Li, W.: '*Applied nonlinear control*' (Prentice-Hall Press, 1991)
[14] Bhardwaj, M.: 'Software phased-locked loop design using C2000™ microcontrollers for single phase grid connected inverter'. Application Report, Texas Instruments, July 2013
[15] IEEE 519 Recommended Practices and Requirements for Harmonic Control in Electrical Power Systems, IEEE Standard, 1993

8 Appendix

8.1 Appendix 1: Averaged state-space model of the system

During active switching state, T_{A^+} and T_{B^-} are tuned on. The filter equivalent circuit is shown in Fig. 1*b*. Assuming $\boldsymbol{X} = (x_1, x_2)^{\rm T} = (i_{\rm F}, v_{\rm DC})^{\rm T}$ as the state vector, the state-space equations can be written as follows:

$$\dot{\boldsymbol{X}} = \boldsymbol{A}_{\rm on}\boldsymbol{X} + \boldsymbol{B}_{\rm on}$$
$$\begin{pmatrix} \dot{x}_1 \\ \dot{x}_2 \end{pmatrix} = \begin{pmatrix} -\dfrac{r_L + 2r}{L} & -\dfrac{1}{L} \\ \dfrac{1}{C} & 0 \end{pmatrix} \begin{pmatrix} x_1 \\ x_2 \end{pmatrix} + \begin{pmatrix} \dfrac{v_s}{L} \\ 0 \end{pmatrix} \tag{27}$$

where r and r_L are equivalent resistances of the power switches coupling reactor, respectively. Similarly, considering Fig. 1*c*, state-spaces equations of the system during inactive switching interval is

$$\dot{\boldsymbol{X}} = \boldsymbol{A}_{\rm off}\boldsymbol{X} + \boldsymbol{B}_{\rm off}$$
$$\begin{pmatrix} \dot{x}_1 \\ \dot{x}_2 \end{pmatrix} = \begin{pmatrix} -\dfrac{r_L + 2r}{L} & +\dfrac{1}{L} \\ -\dfrac{1}{C} & 0 \end{pmatrix} \begin{pmatrix} x_1 \\ x_2 \end{pmatrix} + \begin{pmatrix} \dfrac{v_s}{L} \\ 0 \end{pmatrix} \tag{28}$$

Considering Fig. 1*d*, it is obvious that (27) and (28) are valid for time duration of $t_{\rm on}$ and $t_{\rm off}$, respectively. These could be combined with respect to the averaging technique in the whole switching period. So system model will be $\dot{\boldsymbol{X}} = \boldsymbol{A}_{\rm avg}\boldsymbol{X} + \boldsymbol{B}_{\rm avg}$, where $\boldsymbol{A}_{\rm avg} = (1/T)(t_{\rm on}\boldsymbol{A}_{\rm on} + t_{\rm off}\boldsymbol{A}_{\rm off})$ and $\boldsymbol{B}_{\rm avg} = (1/T)(t_{\rm on}\boldsymbol{B}_{\rm on} + t_{\rm off}\boldsymbol{B}_{\rm off})$ are average values of the state-space matrices. By defining $t_{\rm on} = DT$ and $t_{\rm off} = (1 - D)T$, where

$D \in [0, 1]$ is converter duty cycle, the averaged state-space matrices can be obtained as

$$\boldsymbol{A}_{\text{avg}} = D\boldsymbol{A}_{\text{on}} + (1 - D)\boldsymbol{A}_{\text{off}} = \begin{pmatrix} -\dfrac{r_L + 2r}{L} & -\dfrac{2D - 1}{L} \\ \dfrac{2D - 1}{C} & 0 \end{pmatrix} \tag{29}$$

$$\boldsymbol{B}_{\text{avg}} = D\boldsymbol{B}_{\text{on}} + (1 - D)\boldsymbol{B}_{\text{off}} = \begin{pmatrix} \dfrac{v_s}{L} \\ 0 \end{pmatrix} \tag{30}$$

Due to the presence of $(2D - 1)$ in these equations, control variable can be defined as $u = 2D - 1$ where $u \in [-1, 1]$. Considering the OAB triangle in Fig. 1*d*, the following equation could be written according to Thales' theorem:

$$MN \parallel AB \Rightarrow \frac{ON}{OB} = \frac{MN}{AB} \tag{31}$$

Equation (31) can be rewritten as follows considering Fig. 1*d*:

$$\frac{t_{\text{on}}/2}{T/2} = \frac{v_{\text{control}} + \hat{V}_{\text{tri}}}{2\hat{V}_{\text{tri}}} \Rightarrow D = \frac{1}{2}\left(1 + \frac{v_{\text{control}}}{\hat{V}_{\text{tri}}}\right) \tag{32}$$

or

$$\frac{v_{\text{control}}}{\hat{V}_{\text{tri}}} = 2D - 1 \Rightarrow u = \frac{v_{\text{control}}}{\hat{V}_{\text{tri}}} \tag{33}$$

According to (33), if it is assumed that $\hat{V}_{\text{tri}} = 1$, u, the controller output will be equal to input signal of the PWM unit. Hence, it is possible to connect output of the developed non-linear controller directly into PWM unit.

8.2 Appendix 2: Stability analysis of the proposed controller

To prove convergence of the error variables into zero, the following lemma can be introduced:

Barbalat lemma [13]: Suppose that the scalar function $V(x, t)$ satisfies the following conditions:

i. $V(x, t)$ is a lower bounded function.
ii. $\dot{V}(x, t)$ is a negative semi-definite function.
iii. $\dot{V}(x, t)$ is a uniformly continuous function.
iv. then $\dot{V}(x, t)$ will converge into zero as time increases $(t \to \infty)$.

Since V_2 in (18) satisfies first and second conditions, it is enough to check continuity of the $\dot{V}(x, t)$. For this purpose, time derivative of $\dot{V}(x, t)$ is calculated

$$\ddot{V}_2 = -2c_1 z_1 \dot{z}_1 + \dot{z}_1 z_2 + z_1 \dot{z}_2 - 2c_2 z_2 \dot{z}_2$$

By replacing $\dot{z}_1$ and $\dot{z}_2$ from (14) and (15) in this equation, respectively, and considering that all of the parameters and error variables are bounded, it can be concluded that $\ddot{V}_2$ is a bounded function. As a result, $\dot{V}_2$ would be uniformly continuous. Briefly, application of the Barbalat lemma proves that error variables z_1 and z_2 converge into zero as $t \to \infty$. As a result, proposed adaptive non-linear controller results in asymptotical stability of the system in a wide range of operation.